Adapting a scaled twin-disc device for tread braking investigations based on an ad-hoc thermal similitude model

Wear 574–575 (2025) 206105

Contents lists available at ScienceDirect

Wear

journal homepage: www.elsevier.com/locate/wear

Adapting a scaled twin-disc device for tread braking investigations based on an ad-hoc thermal similitude model

Matteo Magelli, Rosario Pagano, Nicolò Zampieri *

Politecnico di Torino, Department of Mechanical and Aerospace Engineering, C.so Duca degli Abruzzi 24, 10129, Torino, Italy

ARTICLE INFO

Keywords:
Twin-disc
Mechanical design
Tread braking
Similitude model
Finite element method

ABSTRACT

The present paper shows the design of a scaled tread braking system to be included in a scaled twin-disc system, to carry out thermomechanical investigations on wheel and shoe materials. The test bench consists of two discs, pressed against each other, simulating the wheel-rail contact. A pneumatic cylinder pushes scaled brake shoes against the wheel tread surface, and a fan-nozzle device improves convection cooling. As a major novelty, both systems are designed to comply with a new thermal scaling method, that is specifically identified to obtain the same temperature field on the scaled twin-disc as for a full-scale system. The paper thoroughly describes the mathematical background of the new thermal scaling method, which is then preliminarily validated with finite element thermal models for both the brake block and wheel. The greatest advantage of the final twin-disc configuration is that it allows to carry out investigations of wheel-rail wear phenomena as well as studies on the thermomechanical interaction between wheels and brake shoes, while adhering to scaling rules that corroborate the validity of the experimental results.

1. Introduction

Tread braking in railway vehicles works by pressing brake blocks against the wheel tread surface, generating friction that dissipates kinetic energy as heat, thus raising the wheel temperature. The wheel tread simultaneously transfers part of this heat through convection with ambient air and through conduction to the colder rail at the wheel-rail contact patch, a process known as “rail chill” [1]. The repeated cycle of heating and cooling may cause detrimental effects, including microstructural changes near the contact surface and high tensile stresses on the wheel surface [2,3]. These stresses may lead to thermomechanical crack formation on the wheel tread, thus compromising vehicle safety and requiring more frequent wheel profile maintenance. Therefore, a deep understanding of the interaction between railway wheels and brake blocks is essential. Several studies have been carried out to study the damage on railway wheels, and they have been conducted on the field [4], in laboratory environments using full scale [5,6] or small-scale test rigs [7–12] and even via simulated experiments [13–15].

While full-scale testing allows to simulate phenomena with great fidelity and accuracy, they are expensive and not suitable for small laboratory facilities. Alternatively, small-scale benches allow to gather useful insights on the tribological behaviour of wheels, while also maintaining low construction and setup costs. Scaled test rigs however require a scaling strategy to be defined, which is chosen depending on the goals of the experimental activities. In fact, size scaling translates to the scaling of all other physical quantities to ensure compatibility between the scaled system and the full-scale counterpart. This means that to effectively correlate data from scaled test rigs to full-scale systems, a similitude model (or scaling rule) is essential. A detailed mathematical analysis of the derivation of scaling factors relevant to railway dynamics is thoroughly discussed and presented in the review by Bosso et al. [16].

Among the small-scale test rigs commonly used to study the tribological properties of steels used in wheel-rail systems, twin-disc machines have attracted attention from researchers over the last years, as they allow to replicate contact phenomena better than tribometers such as the pin-on-disc and ball-on-disc machines, while still maintaining reduced costs with respect to full-scale and on-field tests [17].

Twin-disc test rigs are usually adopted to analyse a multitude of tribological parameters on the steels used in wheel-rail systems, such as wear rate, crack nucleation and propagation, coefficient of friction (COF) [17–24]. Whilst common twin-disc systems do not comply with specific scaling rules, the railway research group from Politecnico di Torino (PoliTo) recently designed a novel scaled twin-disc device [25] based on Pascal’s similitude model, which allows to obtain the same

* Corresponding author.
E-mail address: nicolo.zampieri@polito.it (N. Zampieri).

https://doi.org/10.1016/j.wear.2025.206105
Received 26 January 2025; Received in revised form 28 March 2025; Accepted 25 April 2025
Available online 26 April 2025

contact pressure as for a full-scale system [16,26]. The main novelty of the test bench is that both the rail and wheel discs are machined to the actual scaled profile shapes, and the lateral rail profile is adjusted to compensate for the longitudinal roller curvature. A detailed description of the original configuration of the novel test rig can be found in Ref. [25]. The novel twin-disc was originally designed to perform wear tests on wheel and rail steels, in order to validate numerical models for the prediction of the wheel and rail profile evolution [27,28]. To investigate thermomechanical phenomena related to the wheel-block contact, the PoliTo research group was initially planning to design and build a separate scaled test bench. However, to optimize costs and minimize laboratory space requirements, it was decided to adapt and upgrade the novel twin-disc. As the bench was originally conceived for wear investigations following Pascal's similitude model, the adaptation required the definition of a different scaling rule for the investigation of thermal phenomena, to ensure a strong correlation between the data gathered from the scaled tests and the real-world scenarios. The present paper shows in detail the derivation of an ad-hoc scaling rule for thermal phenomena and the consequent design of the new components to be installed on the bench to perform tread braking tests with the scaled twin-disc.

The paper is organised as follows. Section 2 describes the original configuration of the novel twin-disc rig designed in past activities by the PoliTo railway research team, which represents the starting point for the upgrades with installation of the scaled tread braking system. Section 3 focuses on the derivation of the new thermal similitude model and on its validation through finite element (FE) analysis. Next, Section 4 describes the design of the scaled tread braking system with scaled shoes based on the design constraints applied by the new thermal scaling rule, and then shows the final configuration of the twin-disc. The final configuration of the scaled twin-disc with the scaled tread braking system allows to execute wear tests as well as to investigate the thermal behaviour caused by tread braking operations. Finally, the Conclusion section summarises the activity that was carried out and discusses other types of tests that can be possibly executed in the future with the upgraded twin-disc configuration.

2. Original design of the bench

The novel twin-disc was originally designed for the investigation of wear at the wheel-rail interface. The bench CAD model is shown in Fig. 1.

The test rig is connected to a rigid frame (1) with a series of bolts. The core components of the twin-disc tribometer are the disc specimens (5) and (6), each driven by a brushless motor (7), allowing to reach the desired creepage between them. Both wheel and rail rollers include a hub (8), which is connected to the corresponding shaft (9). Two steel traction rods (2) connect the upper (3) and lower (4) plates and support the load application system. The latter is based on helical springs (10) which apply the normal load at the contact interface between the rollers, thus reproducing the required axle-load value. These springs, positioned between the loading beam (11) and the upper plate (3), ensure a limited loss of the contact load as profiles wear over time. Additionally, a linear potentiometer (12), mounted parallel to the compression springs, allows to accurately measure the load applied by the system.

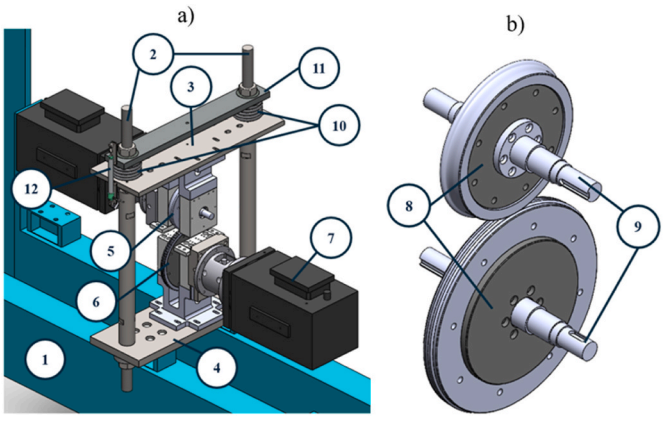

Fig. 1. (a) CAD model of the novel twin-disc tribometer and (b) detail of the wheel and rail rollers. (1) Rigid frame, (2) Traction rods, (3) Upper plate, (4) Lower plate, (5) Wheel disc, (6) Rail disc, (7) Brushless motor, (8) Disc hubs, (9) Disc shafts, (10) Helical springs, (11) Loading beam, (12) Linear potentiometer.

The bench adheres to Pascal's similitude model [16,26], which aims at keeping the same pressure on the scaled and full-scale systems. Table 1 shows the values of the scaling factors according to Pascal's scaling rule for the main quantities of interest, given as a function of the scaling factor for sizes φ_L. The novel bench has a scaling factor for sizes $\varphi_L = 5$, i.e., sizes on the bench are smaller by a factor 5 with respect to the full-scale values.

To also ensure a consistent scaling of the contact area, which is not inherently addressed by Pascal's similitude model, the rail disc profile was modified. In fact, although Pascal's similitude model theoretically allows to keep the same normal pressure in the full-scale and scaled systems, the rail roller features a finite longitudinal curvature, which differs from the infinite longitudinal curvature of a real rail. Therefore, as a major novelty of the new test bench, a change in the lateral curvature of the rail roller profile was performed, to compensate for the roller radius in longitudinal direction.

The bench is designed to perform different types of tests. By controlling the angular speed of each motor and adjusting the normal load, tests can be carried out at different values of creepage, reference speed and contact pressure. The amount of worn material can be measured using a laser system already available in the laboratories of the research group, which will be installed on the bench in future upgrades of the activities. The wear tests will be run to tune wear coefficients adopted in several heuristic wear laws for different operating conditions of railway vehicles [29,30]. Alternatively, adhesion tests can be performed by setting a constant speed for one disc while progressively increasing the resistant torque on the other roller, allowing measurement of adhesion curves in dynamic conditions.

It is believed that the key features of the newly designed bench, namely the use of scaled profiles and the correction of the lateral curvature of the rail disc profile, will allow to derive data that more closely matches real-world operating conditions of railway vehicles.

As an upgrade of the original configuration, the activity shown in the present paper aims at adding a scaled tread braking system on the novel twin-disc. This upgrade enables the investigation of the thermal behaviour of wheels and shoes during the application of braking forces. However, to effectively correlate data from scaled test rigs to full-scale wheel-brake contact, a suitable thermal similitude model is essential.

Table 1
Scaling factors according to Pascal's similitude model.

Quantity	Scaling Factor
Length	φ_L
Density	1
Young's modulus	1
Contact Pressure	1
Area	φ_L^2
Time	φ_L
Speed	1
Acceleration	φ_L^{-1}
Mass	φ_L^3
Force	φ_L^2
Weight	φ_L^3

3. Thermal scaling for drag braking operations

3.1. Derivation of the thermal scaling rule

A novel similitude model must be developed for thermal investigation purposes, considering the constraints represented by design choices previously made to obtain the original bench configuration and due to the original Pascal's similitude model. A novel thermal scaling rule is essential to correlate the results obtained on the scaled test rig to full-scale quantities. The main advantage of employing the novel thermal scaling rule during experimental campaigns is that the thermal field of the scaled components is the same as the one on the full-scale systems. This means that data obtained from experimental tests run with the scaled test rig are indicative of real drag braking scenarios.

According to a well-established literature approach, in this paper the thermal similitude model is obtained by writing the system of partial derivatives differential equations (PDE) governing the thermal problem for the full scale and scaled systems. The idea is to identify a set of non-dimensional groups that should have the same value on the scaled and full-scale systems.

$$\begin{cases} \dot{T} = \dfrac{\lambda}{\rho c}\dfrac{t^*}{L^{*2}}\nabla^2 T, \ \Omega \\ -\lambda\nabla T\cdot\boldsymbol{n} = \Phi_{in}(t), \ \Gamma_1 \\ -\lambda\nabla T\cdot\boldsymbol{n} = U(T_B - T), \ \Gamma_2 \\ T(\boldsymbol{x}, t=0) = T_0(\boldsymbol{x}) \end{cases} \tag{1}$$

If constant thermal properties are considered, thus neglecting the dependency of material properties on temperature, a PDE with prescribed boundary conditions (BCs) and initial conditions (ICs) in the following form can be derived for both the wheel and brake block:

where T is temperature, $\dot{T}$ is the temperature time derivative, t is time, $\mathbf{x}$ is the vector of coordinates defining points belonging to the computational domain Ω, Γ_1 is a domain border where heat flux Φ_{in} is prescribed, Γ_2 is a domain border where convection is prescribed, with fluid temperature T_B and convection coefficient U, T_0 is the function providing the initial temperature field over the domain and finally ρ is density, c is specific heat and λ is thermal conductivity. It can be easily noticed that in Equation (1) the first expression is the diffusion equation, governing the thermal problem in a solid body, the second and third expression state the BCs of prescribed heat flux and convection, respectively, and finally the last expression prescribes the IC in terms of the initial temperature field over the computational domain, i.e., the wheel/brake block.

When considering either a full scale or scaled system, it is possible to identify reference values for the main quantities that appear in the PDE system as stated by Equation (1), so that all the expressions can be rewritten in terms of non-dimensional variables. Therefore, it is possible to define the following normalized quantities:

$$\begin{cases} \overline{T} = \dfrac{T}{T^*} \\ \overline{\boldsymbol{x}} = \dfrac{\boldsymbol{x}}{L^*} \\ \overline{t} = \dfrac{t}{t^*} \\ \overline{\Phi} = \dfrac{\Phi_{in}}{\Phi^*} \\ \overline{U} = \dfrac{U}{U^*} \\ \overline{T_B} = \dfrac{T_B}{T_B{}^*} \end{cases} \tag{2}$$

where the asterisk is used to identify the reference values and the line over each symbol is used to refer to a non-dimensional quantity. By including Equation (2) into Equation (1), it is possible to obtain the following system of PDEs in terms of non-dimensional variables:

$$\begin{cases} \dot{\overline{T}} = \dfrac{\lambda}{\rho c}\dfrac{t^*}{L^{*2}}\overline{\nabla}^2\overline{T}, \ \Omega\overline{\nabla T}\cdot\boldsymbol{n} = -\dfrac{\Phi^* L^*}{\lambda}\overline{\Phi}(t), \ \Gamma_1\overline{\nabla T}\cdot\boldsymbol{n} = -\dfrac{U^* L^*}{\lambda T^*}\overline{U}(T_B{}^*\overline{T_B} - T^*\overline{T}), \ \Gamma_2\overline{T}(\overline{\boldsymbol{x}}, \overline{t}=0) = \overline{T_0}(\overline{\boldsymbol{x}}) \end{cases} \tag{3}$$

From the PDE system written in terms of non-dimensional variables as stated by Equation (3), it is possible to identify the following four non-dimensional groups:

$$\begin{cases} A_1 = \dfrac{\lambda}{\rho c}\dfrac{t^*}{L^{*2}} \\ A_2 = \dfrac{\Phi^* L^*}{\lambda} \\ A_3 = \dfrac{U^* L^* T_B{}^*}{\lambda T^*} \\ A_4 = \dfrac{U^* L^*}{\lambda} \end{cases} \tag{4}$$

among which the reader can observe that A_4 corresponds to the well-known Biot number Bi, i.e., $A_4 = Bi$. Furthermore, in case a reference speed is defined, such that:

$$V^* = \frac{L^*}{t^*} \tag{5}$$

it can be observed that the first non-dimensional group corresponds to the inverse of the Peclet number *Pe*, i.e., $A_1 = Pe^{-1}$.

The identification of the four non-dimensional groups in Equation (4) allows to state that a full-scale and scaled system have the same thermal behaviour if the non-dimensional groups feature the same value on the two systems. This means that if scaling quantities are defined for the non-dimensional groups as:

$$\varphi_{Aj} = \frac{(A_j)_f}{(A_j)_s} \tag{6}$$

where j = 1–4 and subscripts f and s refer to the full-scaled and scaled system respectively, they should be unitary to ensure perfect thermal similarity. Equation (6) allows to relate the scaling of the non-dimensional groups to the scaling factor of the individual quantities appearing on the right-hand side of the expressions in Equation (4). Hence, considering that the scaled wheel and brake blocks are made of the same materials as for the real components, the following expressions hold:

$$\begin{cases} \varphi_{A1} = \dfrac{\varphi_t}{{\varphi_L}^2} \\ \varphi_{A2} = \varphi_\Phi \varphi_L \\ \varphi_{A3} = \dfrac{\varphi_U \varphi_L \varphi_{T_B}}{\varphi_T} \\ \varphi_{A4} = \varphi_U \varphi_L \end{cases} \tag{7}$$

where again φ_Q refers to the scaling factor for the generic quantity Q. Considering that temperature inside the body T and temperature of the ambient air T_B should be scaled according to the same factor, only three scaling factors can be defined, as $\varphi_{A3} = \varphi_{A4} = \varphi_{Bi}$. It is easy to demonstrate that with Pascal's similitude model, see Table 1, the three scaling factors for the non-dimensional quantities are:

$$\begin{cases} \varphi_{A1} = \dfrac{1}{\varphi_L} \\ \varphi_{A2} = \varphi_L \\ \varphi_{Bi} = \varphi_U \varphi_L \end{cases} \tag{8}$$

which hinders a perfect thermal similitude on the scaled bench. However, when using the bench for thermal investigations, less attention will be paid to the wheel-rail contact interaction, and focus will be mostly on the wheel-shoe contact. Therefore, a different similitude model is developed to enable the execution of thermal investigations on the upgraded test bench including scaled brake blocks. Precisely, in this paper, a model that enables perfect thermal scaling for drag braking operations is developed and its validity is proved with finite element (FE) analyses.

In drag braking operations, a braking effort is applied to keep a constant speed over a downhill track section. Drag braking operations are used to assess the thermal capacity of brake blocks and wheels, as the well-known European "TSI Wag" rule [31] defines a reference drag braking scenario. The latter corresponds to the braking power required to keep a constant speed of 70 km/h on a downhill section with slope equal to the one of the Gotthard tunnel on a vehicle with axle load of 22.5 tons, and it should be applied for a total duration of 34 min.

For drag braking operations, a thermal similitude model can be easily defined considering a proper scaling of the thermal flux. A perfect thermal scaling of the diffusion equation can be obtained by applying the braking power for a much shorter time on the scaled bench, such that $\varphi_t = {\varphi_L}^2$. This scaling is different from Pascal's model, that prescribes a scaling factor of time equal to the scaling factor of length, but it allows to obtain a unitary factor for the first non-dimensional group, i.e., $\varphi_{A1} = 1$. Similarly, if the applied thermal flux is amplified on the scaled test bench, such that $\varphi_\Phi = \frac{1}{\varphi_L}$, then the second non-dimensional number has a unitary scaling, namely $\varphi_{A2} = 1$. Finally, to obtain a unitary scaling for the last non-dimensional group, i.e., the Biot number, the convection coefficient should be magnified on the scaled twin-disc bench such that $\varphi_U = \frac{1}{\varphi_L}$. The main design challenges for a perfect scaling of the thermal behaviour in drag braking operations are hence represented by the need for an amplification of the thermal flux and of the convection coefficient.

The average thermal flux generated by friction at the wheel-shoe contact interface can be calculated as:

$$\Phi_{ws} = \frac{\mu F_s V}{L_s H_s} \tag{9}$$

where μ is the friction coefficient, F_s is the shoe pressing force, V is the wheel linear speed, L_s is the shoe circumferential length and H_s is the shoe axial width. By writing Equation (9) above for both the full-scale and scaled systems, and neglecting the scaling of the friction coefficient, the scaling factor for the flux can be calculated as:

$$\varphi_\Phi = \frac{\varphi_{Fs} \varphi_V}{{\varphi_L}^2} \tag{10}$$

As time scales as $\varphi_t = {\varphi_L}^2$, a consistent scaling of speeds would require $\varphi_V = \frac{1}{\varphi_L}$, i.e., speed should be amplified on the scaled twin-disc bench. However, this would lead to huge values of rotational speeds of the wheel and rail discs, that are not compatible with the electric motors available at the laboratories of the research group and installed on the novel twin-disc. Furthermore, the design of a speed multiplier is not an option as very high rotational speeds could represent a concern in terms of safety. To tackle this issue, an inconsistent scaling of speed is performed, by setting $\varphi_V = 1$, thus leaving this factor unchanged with respect to the standard Pascal's stating strategy. Hence, to achieve $\varphi_\Phi = \frac{1}{\varphi_L}$, the shoe pressing force should be scaled such that $\varphi_{Fs} = \varphi_L$, which differs from Pascal's similitude scaling, that prescribes a scaling factor of forces $\varphi_F = {\varphi_L}^2$. Please note that with this inconsistent scaling of speed, it is still possible to scale drag braking operations, where the braking effort is unchanged for the whole duration of the operation, while it is not possible to achieve a perfect thermal similitude in stop braking operations, that would require the scaling factors for speed and acceleration to be consistent with the scaling factors defined for length and time. Therefore, the scaling strategy adopted for drag braking operations cannot be extended to stop braking operations. In fact, the perfect scaling of the diffusion equation would lead to $\varphi_V = \frac{1}{\varphi_L}$, which is impossible to achieve with the motors installed on the bench. Therefore, at this stage of the activity, focus is mainly addressed to the perfect similarity of drag braking operations. Table 2 shows the scaling factors for the relevant quantities in thermal tests for both the original Pascal's model and the new thermal scaling rule.

Future upgrades of the activity will deal with the identification of a non-linear correlation of the temperature values recorded on the bench with full-scale data for stop braking operations. Stop braking tests will be carried out using the default Pascal's similitude model to ensure consistency of length, speed and time scaling factors. The nonlinear correlation between the measurements obtained on the scaled system and the corresponding quantity for a full-scale system will be derived thanks to the interpolation of the results of FE thermal models of wheel and shoe shown in the following section.

Table 2
Comparison between Pascal scaling factors and the novel similitude novel scaling factors (*the scaling factor for speed is inconsistent with the scaling factors for length and time, as it is incompatible with the current laboratory limitations).

Quantity	Pascal Scaling rule	Novel Scaling rule
Length	φ_L	φ_L
Area	${\varphi_L}^2$	${\varphi_L}^2$
Time	φ_L	${\varphi_L}^2$
Speed	1	1*
Force	${\varphi_L}^2$	φ_L
Weight	${\varphi_L}^3$	${\varphi_L}^3$
Flux	1	${\varphi_L}^{-1}$
Thermal energy	${\varphi_L}^3$	${\varphi_L}^3$
Convection coefficient	Not addressed	${\varphi_L}^{-1}$
Temperature	Not addressed	1

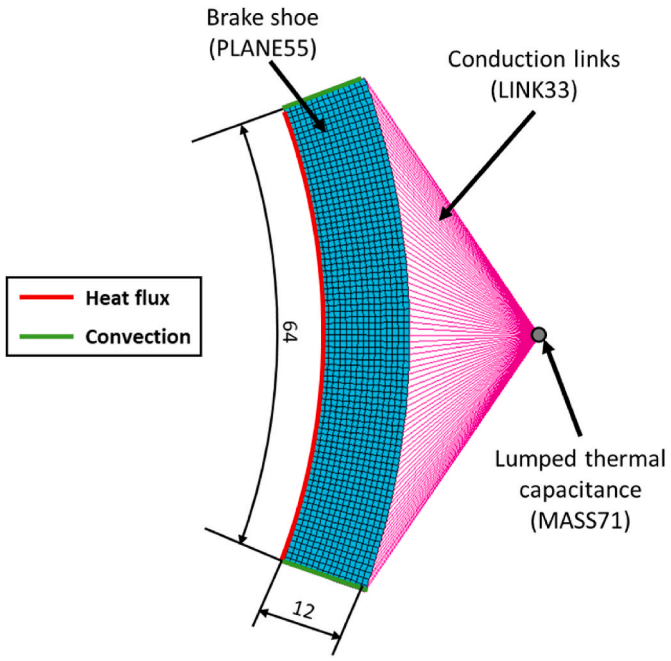

Fig. 2. Plane FE model of the brake block (dimensions given for the scaled system in mm).

3.2. Numerical validation of the thermal scaling rule

To validate the developed thermal scaling rule, FE models are developed to run transient analysis of drag braking operations for both the wheel and brake block. The FE models are developed in the ANSYS Mechanical APDL environment, with APDL scripts that allow to easily switch between a full-scale simulation and a scaled one by applying the scaling factors defined in the previous subsection for the new thermal scaling rule, see Table 2.

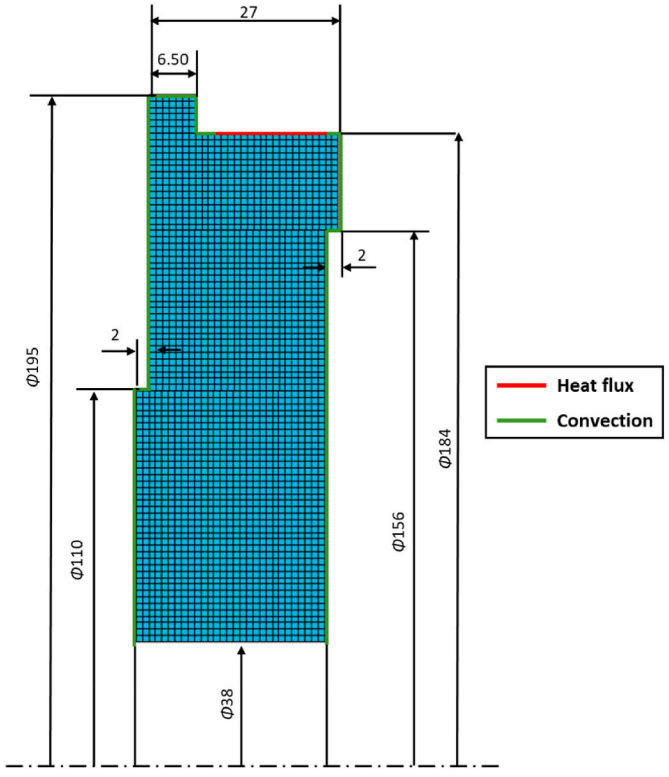

Fig. 3. Plane axisymmetric FE model of the wheel (dimensions given for the 1:5 scaled system in mm).

The FE model for the brake block, shown in Fig. 2 with dimensions for the 1:5 scaled system, is a plane model, that considers the temperature field in the radial and circumferential coordinates. As the FE model is built with the aim of validating the scaling technique rather than to accurately calculate the temperature values, a simplified geometry is considered, and the shoe is modelled as a circular sector, meshed with ANSYS PLANE55 thermal elements. Furthermore, the plane model allows to speed up the simulation times with respect to 3D models [32]. This design corresponds to the actual brake shoe used in the test bench and aligns with the dimensions of brake shoes commonly employed in railway vehicles with Bg brake block configurations. The brake block holder is modelled in a simplified manner, as a lumped thermal capacitance (MASS71) connected to the outer surface of the shoe through conduction links (LINK33). A heat flux is applied to the side of the brake shoe in contact with the wheel, while a convective BC is applied on the upper and lower faces.

On the other hand, the FE thermal model of the wheel, shown in Fig. 3 with dimensions in mm for the scaled system, is built as a plane axisymmetric model, hence neglecting the temperature variation along the circumferential direction, using a solid approach in the literature [33,34]. Again, since this paper aims to validate the derived thermal scaling rule, the geometry is obtained as a simplified version of the actual scaled wheel disc, to simplify meshing operations. A heat flux is prescribed on the tread surface, while a convection BC is prescribed on all free surfaces, see again Fig. 3.

The scaled tread braking system to be included in the twin-disc test rig is designed to be equipped with scaled brake shoes made of any desired material of interest, ranging from traditional P10 cast iron to new engineered composite materials. However, for the sake of validating the novel thermal scaling rule, the FE simulations shown in this paper are run for P10 cast iron shoes. In fact, cast iron is the traditional material adopted for brake shoes, hence solid data about its physical and thermal properties can be found in the literature. Conversely, the properties of composite shoes have a wider variability and depend on the specific considered engineered product. Precisely, Table 3 provides the reference values of the main material properties of the wheel and cast iron brake shoe adopted in a first set of FE simulations, run with constant material properties. An additional set of simulations is run considering the temperature-dependent behaviour of both materials, using polynomial regressions obtained from the experimental data provided by Vernersson et al. [34]. The trend of the polynomial regressions is shown in Fig. 4.

For both models, transient simulations are run for a 2Bg block configuration considering the aforementioned TSI Wag reference drag braking operation of a 22.5-ton axle-load vehicle running at 70 km/h on a downhill slope of 21 ‰. Th average friction heat flux at each wheel-shoe contact interface on the full-scale system can be calculated as:

$$(\Phi_{ws})_f = \frac{Q_{ax}}{2 \cdot N_b} \cdot g\, i_s V \cdot \frac{1}{L_s H_s} \tag{11}$$

where Q_{ax} is the reference vehicle axle-load, g is the gravity, i_s is the reference downhill slope, V is the reference speed and N_b is the number

Table 3
Thermal properties of the brake shoes and wheel, used in the FE simulations.

	Brake shoe (cast iron P10)	Wheel (Steel)	Unit of measurement
λ (thermal conductivity)	48	50	$\frac{W}{m\,K}$
ρ (density)	7100	7818	$\frac{kg}{m^3}$
c (specific heat)	500	487	$\frac{J}{kg\,K}$

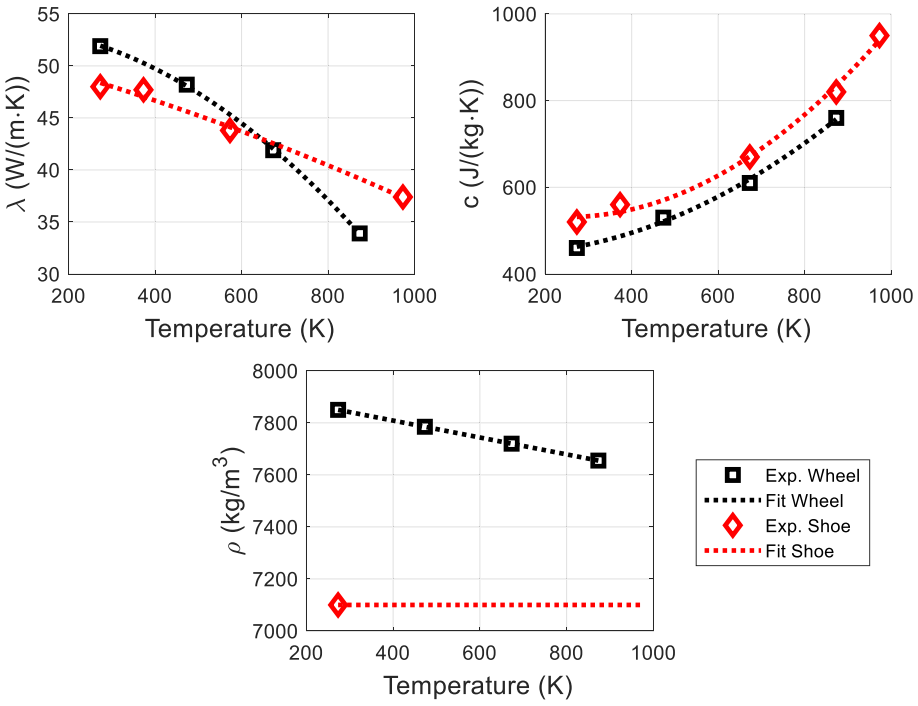

Fig. 4. Polynomial regression of temperature-dependent parameters for brake shoes and wheel.

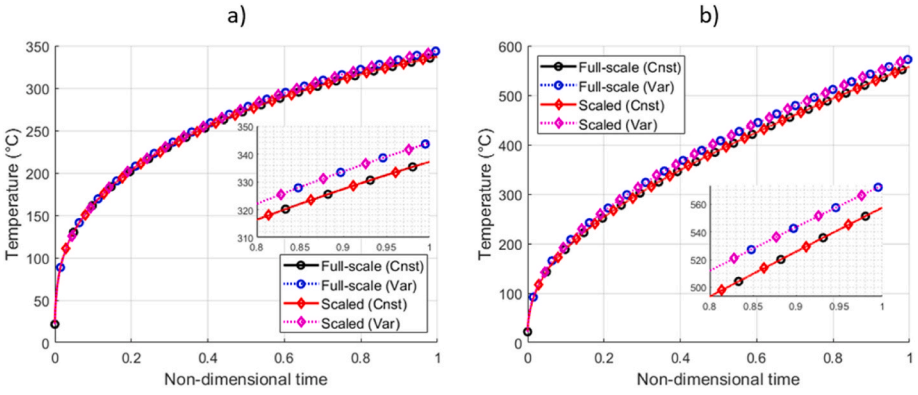

Fig. 5. Temperature evolution of the reference nodes on a) wheel model and b) brake block FE model for full-scale and scaled systems.

of brake blocks per wheel. The total heat flux is partitioned between wheel and shoe according to a partitioning factor β, as:

$$\begin{aligned} \Phi_w &= \Phi_{ws} \cdot \beta \\ \Phi_s &= \Phi_{ws} \cdot (1-\beta) \end{aligned} \tag{12}$$

where subscripts w and s refer to wheel and shoe, respectively. The partitioning factor can be calculated from literature equations as a function of wheel and shoe material properties [35,36] and brake block configuration. For the considered operating scenario, the total heat flux generated by friction at each wheel-shoe contact is 880170 W/m^2 on the full-scale system. Since the partitioning factor is estimated around 81.90 %, for each contact interface, a heat flux of 720849 W/m^2 flows towards the wheel, while the remaining heat flux of 159320 W/m^2 enters the brake block.

Fig. 5a shows the evolution of temperature for a node located in the middle of the wheel tread, while Fig. 5b plots the temperature of a node in the middle of the block inner surface. To simplify the comparison, the x-axis is non-dimensional, i.e., for the full-scale and scaled systems, time is divided by the simulated time, which is 34 min for the full-scale system and 81.6 s for the scaled one. In both plots, the results are given for the full-scale and scaled systems for the two types of simulations, namely simulations run with application of constant material parameters, see Table 3, and simulations run considering the dependency of wheel and brake block material parameters on temperature, see Fig. 4.

It can be observed that the results of the scaled system align perfectly with the output obtained on the full-scale system for both types of simulations, thus proving the validity of the derived thermal scaling rule. For both the wheel and brake block, it can be observed that a higher temperature is obtained when considering the thermal dependency of material parameters. This is because according to the aforementioned literature data, at higher temperature, the thermal conductivity decreases, while the thermal capacity tends to increase, see Fig. 4.

To further prove the validity of the thermal scaling rule, Fig. 6 provides the temperature field in the wheel at the end of the drag braking operation, while Fig. 7 shows the final temperature field in the block. For the sake of brevity, these results are given for the simulations with constant material parameters only, but the same conclusions can be drawn from simulations accounting for the thermal dependant behaviour. In fact, since temperature has a unitary scaling factor with the

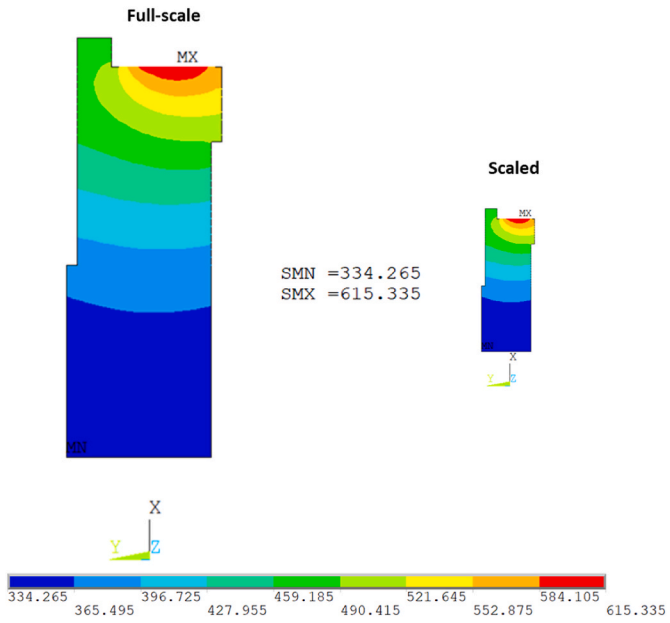

Fig. 6. Temperature field at the end of the drag braking operation for the full-scale and scaled wheel FE models (values in K).

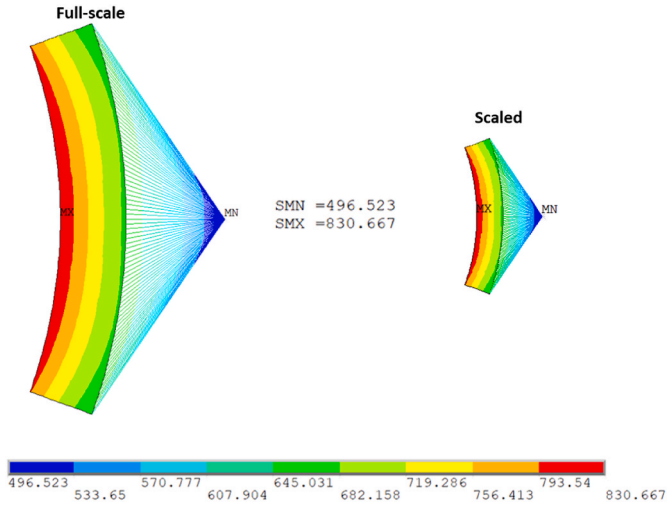

Fig. 7. Temperature field at the end of the drag braking operation for the full-scale and scaled brake block FE models (values in K).

novel thermal scaling rule, the non-linear dependency of material properties on temperature do not compromise scaling. It can be observed from Figs. 6 and 7 that not only the temperature on the reference nodes is well aligned, but also the same temperature field is produced on the two systems. Therefore, it is concluded that the proposed thermal scaling can effectively be used to simulate drag braking operations on the scaled system, allowing to easily correlate data obtained from scaled tests to the corresponding quantities on a full-scale system.

It should be noted that while these simulations were run using the materials listed in Table 3, the effectiveness of the thermal scaling rule does not depend on the adopted materials. In fact, the scaling rule does not require changes in the material properties on the scaled system and ensures that temperature values on the scaled and full-scale systems is the same. The thermal properties of the materials used in the FE model have been extensively investigated in the literature, therefore their values can be easily determined. On the other hand, the properties of composite materials for railway brake shoes strongly depend on the specific product and are overall more variable. Nonetheless, the similitude model is valid regardless of the material and brake shoes made of composite materials will be among the ones investigated using the updated test bench. However, as the thermal similitude model prescribes higher contact pressures, depending on the composite material used, some axle load-braking pressure combination might not be feasible as they could exceed the composite material tensile strength.

4. New design

The twin-disc was upgraded to include a scaled tread braking system, designed based on the novel thermal scaling rule shown in the previous section. Namely, this required finding a brake application system capable of producing a pressing force scaled a factor φ_L and a system that increases the air speed to achieve the desired convection coefficient, which is scaled by $\varphi_U = \frac{1}{\varphi_L}$, see Table 2.

The modified scaling factor for wheel-shoe pressing forces, namely setting $\varphi_{Fs} = \varphi_L$, poses some constraints on the design of the pneumatic brake cylinder that is used to press the brake shoes against the wheel tread surface on the novel twin-disc. The pressing force on a full-scale tread braked wheel in a drag braking operation can be estimated from a wheel rotational equilibrium as:

$$(F_s)_f = \frac{Q_{ax}}{2}\frac{g i_s}{\mu N_B} \tag{13}$$

where Q_{ax} is the vehicle axle-load, g is gravity, i_s is the track downhill slope and N_B is the number of blocks per wheel. Considering the operating conditions of the reference scenario defined in international rules and recognizing that the critical configuration is with a single block per wheel, with the assumption of a value $\mu = 0.2$, that is in the range of

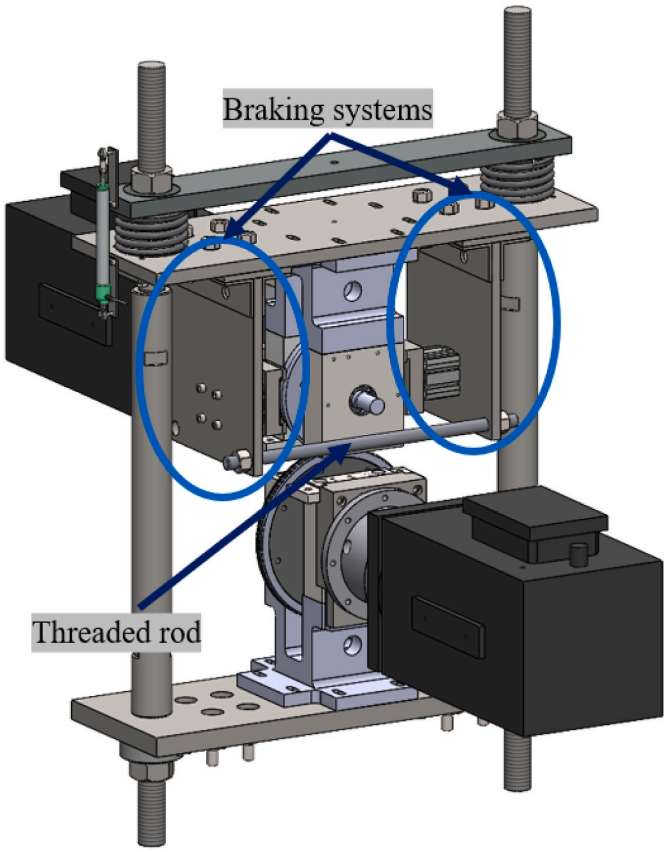

Fig. 8. CAD model of the test rig including braking systems on both sides of the wheel.

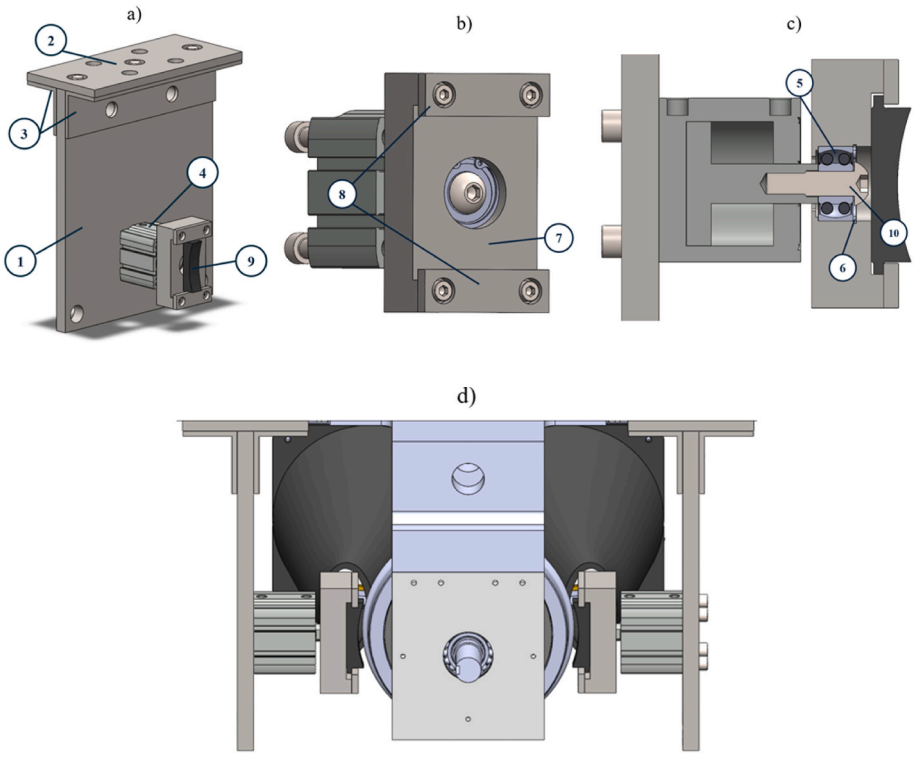

Fig. 9. (a) CAD Model of the braking system (b) Detail of the piston and brake shoe housing (c) Cross section view of the piston and brake shoe housing. (d) Detail of the brake shoes in position. (1) Vertical plate, (2) Horizontal plate, (3) Gussets, (4) Pneumatic cylinder, (5) Self-aligning ball bearing, (6) Circlip, (7) Housing plate, (8) Small plate, (9) Brake shoe, (10) Screw.

both traditional P10 shoes and innovative composite materials, the pressing force on the full-scaled system is equal to 11.6 kN. Therefore, the force on the scaled system is equal to approximately 2.3 kN. To apply this force, the FESTO ADN-S-50-25-I-P-A pneumatic cylinder is selected considering that the maximum air pressure that can be applied by the pneumatic circuit in the laboratories of the research group is limited to 10 bar and considering additional dimensional and mounting constraints.

The new configuration of the scaled twin-disc device includes two braking systems, each mounted on the sides of the wheel-disc in order to perform both 1Bg and 2Bg test configurations, as shown in Fig. 8.

The detailed CAD model of the newly designed tread braking system is shown in Fig. 9. Each system consists of the same components: two plates, a vertical one (1) and a horizontal one (2), two gussets (3), a pneumatic cylinder (4), a self-aligning ball bearing (5), a circlip (6), a housing plate for the brake (7), two small plates (8) that fix the block to the housing and finally the scaled brake shoe itself (9). Please note that Fig. 9d includes the design of a fan cooling system, which will be described in depth below.

Each system is mounted to the upper plate of the main rig via the horizontal plate (2) and bolts, passing through slotted holes that enable minor adjustments along the brake shoe pressing direction. The braking system is mounted on the vertical plate (1), which is secured with screws and gussets, providing rigidity and minimizing relative motion between the braking system and the rest of the bench. The vertical plate (1) features two holes at the bottom, which can be used to include a threaded rod, to minimize the plate deformation, see Fig. 8. The brake cylinder (4) is bolted to the lower part of the vertical plate (1), with screws passing through slotted holes to allow for small lateral adjustments to ensure that the brake block is in contact with the wheel tread. The piston rod of the pneumatic brake cylinder (4) pushes the scaled brake shoe (10) against the wheel tread surface. The brake shoe lays on the housing plate (7), and its position is fixed by means of screws used to mount a couple of small plates (8) to the housing plate (7). The system is designed so that the shoes can be easily mounted and dismounted, thus allowing to possibly test different materials, ranging from cast-iron to different types of composite shoes. To ensure contact even after the profiles of shoe and wheel are worn out, a self-aligning ball bearing (5) is mounted between the housing plate (7) and a screw (10), with the latter tightened to the brake cylinder piston rod (4). The inner ring of the self-aligning ball bearing (5), integral with the screw (10), is axially located by a shoulder on the piston rod and a washer placed below the screw head. The outer ring, instead, is integral with the housing plate (7), and the axial position is fixed by a shoulder and a circlip (6). The use of the self-aligning ball bearing (5) allows the brake block to make small rotational adjustments on the wheel disc axis. This allows the brake to adapt to the profile of the wheel, so that the two surfaces can easily match, especially after initial wear of the components.

During both drag and stop braking tests, only a single motor is required, as slip between the two discs will be kept to a minimum to avoid damage of the wheel and rail rims. The system will be powered by the AC motor installed on the rail disc shaft. In drag braking operations, the motor will be controlled to provide a torque balancing the torque produced by the braking system on the wheel disc shaft. On the other hand, for stop braking operations, the motor will be controlled in speed to obtain the desired braking curve based on the applied braking torque. Therefore, this removes the need for a second motor, freeing space to another system, mounted on top of the upper plate. This system, equipped with two fans, allows to control the air flow and thus obtain an increased convection coefficient, as required by the new thermal similitude model, see Table 2.

As stated above, perfect thermal scaling of the thermal problem would require increasing the convection coefficient on the scaled system by $\varphi_U = \frac{1}{\varphi_L}$. The convection coefficient is probably the parameter affected by the largest uncertainty in thermal problems, and it is usually estimated from experimental correlations as a nonlinear function of the well-known Prandtl (Pr) and Reynolds (Re) non-dimensional groups. For wheel and shoes, the following literature correlation [37,38] can be

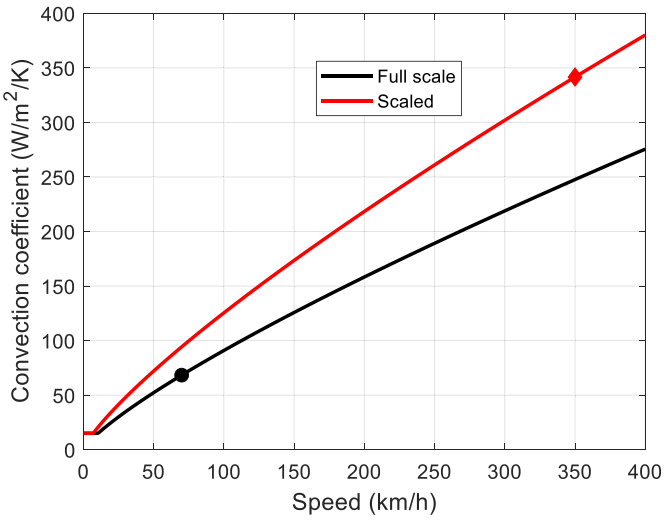

Fig. 10. Convection coefficient for the Full scale and Scaled system vs. vehicle speed.

adopted:

$$U = \frac{0.037\lambda_{air}}{2R_w} Re^{0.8}\, Pr^{0.33} \tag{14}$$

$$Re = \frac{2R_w V \rho_{air}}{\mu_{v,air}}, Pr = \frac{c_{air}\mu_{v,air}}{\lambda_{air}} \tag{15}$$

where R_w is the wheel radius, subscript air refers to ambient air properties, ρ, c and λ are used again for density, specific heat and thermal conductivity, and finally μ_v is the dynamic viscosity. Equations (17) and (18) can be applied to both full-scale and scaled systems, obtaining the trends shown in Fig. 10.

It can be observed that speed should increase approximately by a factor 5 to achieve the desired increase of convection coefficient on the scaled twin-disc rig. Of course, changing the rotational speed of the discs is not feasible. Therefore, a fan system, shown in Fig. 11a, is designed to provide air flow, improving the convection cooling. The system relies on a plate (1), secured to the top of the upper plate of the bench frame, using the existing bolts from the wheel support. The plate (1) is partially bent in a 90° angle to point the airflow directly towards the brake block. By installing the fans (2) in the free space, on the opposite side of the wheel flange, it is possible to cool the contact point of the wheel as well. The selected fans (2) are Orion Fans OD180APL-24H*B series, which are mounted side by side on the bent section of the plate (1), where two holes allow air intake. Using fans of a compact size requires the addition of a convergent nozzle (3), installed in front of the fan and designed to further accelerate the airflow. The nozzle (3), designed using standard fluid machinery equations, accelerates the air and directs it precisely to the brake block, due to the elliptical shape of the nozzle outlet section.

From the theory of ideal nozzle expansion for a subcritical flow, the mass flow rate $\dot{M}$ of air flowing inside the nozzle is given by the following equation:

$$\dot{M} = A_o \sqrt{2 \cdot \frac{\gamma}{\gamma - 1} \cdot \rho_i^t p_i^t \cdot \left[\left(\frac{p_o}{p_i^t} \right)^{\frac{2}{\gamma}} - \left(\frac{p_o}{p_i^t} \right)^{\frac{\gamma+1}{\gamma}} \right]} \tag{16}$$

Where A is the area of the cross section of the nozzle, γ is the heat capacity ratio for air, ρ is density, p is pressure, the subscripts i and o represent respectively the conditions on the inlet and outlet of the pipe, and the superscript t represents the total conditions. The equations used to design the nozzle, including the conservation of mass and the ideal gas law are as follows:

$$\begin{cases} \dot{M} = \rho A v \\ \dfrac{p}{\rho} = R^* \cdot T \\ T^t = T + \dfrac{v^2}{2c_p} \\ \dfrac{p}{\rho^\gamma} = cost \end{cases} \tag{17}$$

where v is the fluid speed, R* is the specific gas constant for air and c_p is the specific heat capacity at constant pressure. By setting the pressure of the air at the outlet of the nozzle and its speed to the desired value, a value for the area of the cross section is obtained. Despite the back-pressure created by the nozzle, the chosen fan is sufficiently powerful to maintain the required airflow.

The updated twin-disc bench will be adopted for both wheel-rail wear studies and investigations into the thermomechanical behaviour of wheel and brake shoe materials such as cast iron and composites. The experimental campaign aiming to investigate the thermal behaviour of wheel and shoes will be run considering different values of braking force and rotational speed, for different shoe materials and block configurations. Data collected from the tread braking tests will be used to calibrate the test rig, as well as to refine, tune and validate the developed FE models. Drag braking tests, run in both 1Bg and 2Bg configurations, will adhere to the proposed thermal scaling rule, with the rail disc, powered by its brushless motor, driving the wheel-disc. Rotational speed and torque values will be recorded via the motor drive, while the brake shoe and wheel roller temperatures will be measured using a thermal imaging camera and thermocouples. The planned experimental campaign will lead the path towards gaining further understanding of the thermal behaviour of wheels and brake blocks comparing different shoe

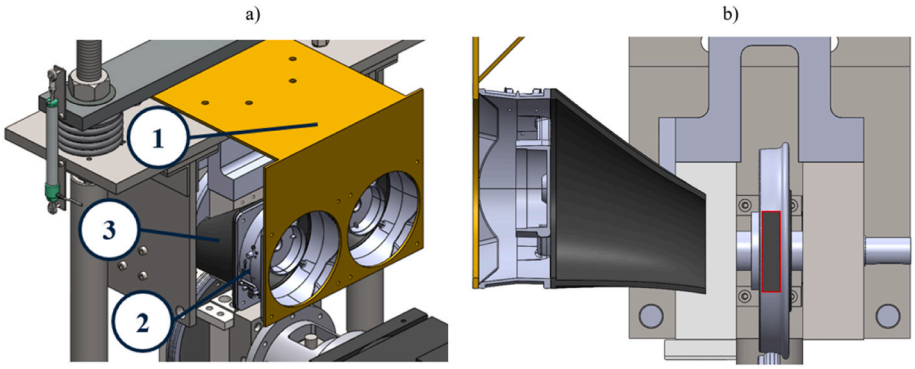

Fig. 11. (a) CAD model of the fan system (b) Cross section view of the fan system aiming at the brake shoe, highlighted in red. (1) Plate, (2) Fans, (3) Nozzles. (For interpretation of the references to colour in this figure legend, the reader is referred to the Web version of this article.)

materials.

5. Conclusions

A scaled tread braking system was designed as an upgrade to the novel twin-disc bench previously designed by the Politecnico di Torino railway research team. The activity focused on the development of ad-hoc thermal scaling rule and its validation through FE analysis. The main outcomes of the activity are given in the following bulleted list.

- A thermal scaling rule for drag braking operations was derived to make sure that the thermal field obtained on the scaled twin-disc rig is identical to the one of a full-scale system. FE simulations proved the effectiveness of the derived thermal scaling rule.
- The thermal scaling rule requires that, when sizes are scaled by a factor φ_L, the heat flux and convection coefficient should both be scaled by a factor ${\varphi_L}^{-1}$, while time should be reduced by a factor ${\varphi_L}^{2}$.
- The scaled tread braking system was designed to comply with the newly conceived thermal scaling rule. The derived thermal scaling factors were used to select the proper pneumatic cylinder, that is able to apply the desired pressing force, and to design the fan-nozzle system that increases convection cooling coefficient on the scaled bench.
- The final configuration of the twin-disc test bench allows to investigate the thermomechanical properties of wheel, rail and brake block materials. Namely, the bench, which previously could only be used to carry out wheel-rail wear tests, was improved as it now allows to conduct brake thermal tests as well.

The new thermal scaling rule cannot be directly extended to stop braking operations, since this would require the scaling factors for speed and acceleration to be consistent with those for time and length, which is incompatible with the adopted motors and could represent a risk in term of safety. Therefore, future developments of the activity will focus on extending tests to stop braking operations, identifying a non-linear correlation between the data obtained from experimental scaled tests and full-scale braking operations. The stop braking tests will be run following Pascal's scaling rule, which keeps a unitary scaling factor for speed, and the non-linear correlation will be derived from an interpolation of the results of FE simulations run with the models developed in this paper, which are going to be validated and tuned against data collected in experimental tests.

CRediT authorship contribution statement

Matteo Magelli: Writing – original draft, Validation, Conceptualization. **Rosario Pagano:** Writing – original draft, Validation, Conceptualization. **Nicolò Zampieri:** Writing – review & editing, Validation, Supervision, Conceptualization.

Declaration of competing interest

The authors declare that they have no known competing financial interests or personal relationships that could have appeared to influence the work reported in this paper.

Data availability

No data was used for the research described in the article.

References

[1] D. Peng, R. Jones, T. Constable, An investigation of the influence of rail chill on crack growth in a railway wheel due to braking loads, Eng. Fract. Mech. 98 (2013) 1–14.

[2] A. Mazzù, L. Provezza, N. Zani, C. Petrogalli, A. Ghidini, M. Faccoli, Effect of shoe braking on wear and fatigue damage of various railway wheel steels for high speed applications, Wear (2019) 434–435.

[3] M.R. Aulia Putra, P.S. Pratama, A.R. Prabowo, Failure of friction brake components against rapid braking process: a review on potential challenges and developments, Transp. Res. Procedia 55 (2021) 653–660.

[4] M.S. Walia, T. Vernersson, R. Lundén, F. Blennow, M. Meinel, Temperatures and wear at railway tread braking: field experiments and simulations, Wear 440–441 (2019).

[5] M.S. Walia, T. Vernersson, K. Handa, K. Ikeuchi, R. Lundén, Wear and plastic deformation of the wheel tread at block braking Results from brake rig experiments and simulations, 19th International Wheelset Congress, Venice, Italy 144 (2019).

[6] M. Faccoli, N. Zani, A. Ghidini, C. Petrogalli, Tribological behavior of two high performance railway wheel steels paired with a brake block cast iron, Tribol. Trans. 65 (2022) 296–307.

[7] N. Bosso, A. Gugliotta, M. Magelli, N. Zampieri, Experimental setup of an innovative multi-axle roller rig for the investigation of the adhesion recovery phenomenon, Exp. Tech. 43 (2019) 695–706.

[8] M. Faccoli, L. Provezza, C. Petrogalli, A. Ghidini, A. Mazzù, A small-scale experimental study of the damage due to intermittent shoe braking on the tread of high-speed train wheels, Tribol. Trans. 63 (2020) 1041–1050.

[9] P. Monreal-Perez, D. Elduque, D. López, I. Sola, J. Yaben, I. Clavería, Full-scale dynamometer tests of composite railway brake shoes including latxa sheep wool fibers, J. Clean. Prod. 379 (2022).

[10] I. Bodini, C. Petrogalli, M. Faccoli, A. Mazzù, Vision-based damage analysis in shoe-braking tests on railway wheel steels, Wear (2022) 510–511.

[11] C. Felhő, G. Hegedűs, L. Kuzsella, K. Voith, D. Drees, Experimental investigations of the wear behaviour of railway brake block raw materials, J. Phys. Conf. 2848 (2024).

[12] L. Ghidini, A. Mazzù, M. Faccoli, Experimental study of wear and rolling contact fatigue in railway wheel steels coupled with various brake block materials: insights from innovative small-scale testing, Wear 558–559 (2024).

[13] T. Vernersson, R. Lunden, S. Abbasi, U. Olofsson, Wear of Railway Brake Block Materials at Elevated Temperatures: Pin-On-Disc Experiments, 2012. Eurobrake 2012, Dresden (Germany).

[14] M. Faccoli, N. Zani, A. Ghidini, C. Petrogalli, Experimental and numerical investigation on the wear behavior of high performance railway wheel steels paired with various brake block materials under dry sliding conditions, Wear 506–507 (2022).

[15] B. White, Z.S. Lee, R. Lewis, Towards a standard approach for the twin disc testing of top-of rail friction management products, Lubricants 10 (2022).

[16] N. Bosso, P. Allen, N. Zampieri, Scale testing theory and approaches, in: S. Iwnicki, M. Spiryagin, C. Cole, T. McSweeney (Eds.), Handbook of Railway Vehicle Dynamics, CRC Press, Boca Raton (FL, USA), 2019, pp. 825–867.

[17] R.C. Rocha, H. Ewald, A.B. Rezende, S.T. Fonseca, P.R. Mei, Using twin disc for applications in the railway: a systematic review, J. Braz. Soc. Mech. Sci. Eng. 45 (2023).

[18] S.R. Lewis, R. Lewis, G. Evans, L.E. Buckley-Johnstone, Assessment of railway curve lubricant performance using a twin-disc tester, Wear 314 (2014) 205–212.

[19] W.J. Wang, S.R. Lewis, R. Lewis, A. Beagles, C.G. He, Q.Y. Liu, The role of slip ratio in rolling contact fatigue of rail materials under wet conditions, Wear 376–377 (2017) 1892–1900.

[20] R. Lewis, E. Magel, W.-J. Wang, U. Olofsson, S. Lewis, T. Slatter, A. Beagles, Towards a standard approach for the wear testing of wheel and rail materials, Proc. Inst. Mech. Eng. F J. Rail Rapid Transit 231 (2017) 760–774.

[21] W.T. Zhu, L.C. Guo, L.B. Shi, Z.B. Cai, Q.L. Li, Q.Y. Liu, W.J. Wang, Wear and damage transitions of two kinds of wheel materials in the rolling-sliding contact, Wear 398–399 (2018) 79–89.

[22] J.F. Santa, P. Cuervo, P. Christoforou, M. Harmon, A. Beagles, A. Toro, R. Lewis, Twin disc assessment of wear regime transitions and rolling contact fatigue in R400HT – E8 pairs, Wear (2019) 432–433.

[23] H. Al-Maliki, A. Meierhofer, G. Trummer, R. Lewis, K. Six, A new approach for modelling mild and severe wear in wheel-rail contacts, Wear 476 (2021).

[24] Y. Hu, W.J. Wang, M. Watson, K. Six, H. Al-Maliki, A. Meierhofer, R. Lewis, Wear of driving versus driven discs in a twin disc rolling-sliding test, Wear 512–513 (2023).

[25] M. Magelli, R. Pagano, N. Zampieri, Design of an innovative twin-disc device for the evaluation of wheel and rail profile wear, Design 8 (2024).

[26] A. Jaschinski, H. Chollet, S. Iwnicki, A. Wickens, J. Würzen, The application of roller rigs to railway vehicle dynamics, Veh. Syst. Dyn. 31 (1999) 345–392.

[27] N. Bosso, N. Zampieri, Numerical stability of co-simulation approaches to evaluate wheel profile evolution due to wear, Int. J. Real. Ther. 8 (2020) 159–179.

[28] M. Magelli, N. Zampieri, Calculation of wear of railway wheels with multibody codes: benchmarking of the modelling choices, Machines 12 (2024).

[29] R. Enblom, Deterioration mechanisms in the wheel–rail interface with focus on wear prediction: a literature review, Veh. Syst. Dyn. 47 (2009) 661–700.

[30] N. Bosso, M. Magelli, N. Zampieri, Simulation of wheel and rail profile wear: a review of numerical models, Railway Eng. Sci. 30 (2022) 403–436.

[31] Commission Regulation (EU), No 321/2013 of 13 March 2013 Concerning the Technical Specification for Interoperability Relating to the Subsystem 'rolling Stock — Freight Wagons' of the Rail System in the European Union and Repealing Decision 2006/861/EC, 2013.

[32] A. Somà, M. Aimar, N. Zampieri, Simulation of the thermal behavior of cast iron brake block during braking maneuvers, Appl. Sci. 11 (2021).

[33] T. Vernersson, Temperatures at railway tread braking. Part 1: modelling, Proc. Inst. Mech. Eng. F J. Rail Rapid Transit 221 (2007) 167–182.

[34] T. Vernersson, Temperatures at railway tread braking. Part 2: calibration and numerical examples, Proc. Inst. Mech. Eng. F J. Rail Rapid Transit 221 (2007) 429–441.
[35] M.R.K. Vakkalagadda, K.P. Vineesh, V. Racherla, Estimation of railway wheel running temperatures using a hybrid approach, Wear 328–329 (2015) 537–551.
[36] N. Bosso, L. Cantone, G. Falcitelli, R. Gjini, M. Magelli, F.M. Nigro, E. Ossola, N. Zampieri, Simulation of the thermo-mechanical behaviour of tread braked railway wheels by means of a 2D finite element model, Tribol. Int. 178 (2023).
[37] M. Milošević, D. Stamenković, M. Tomić, A. Milojević, M. Mijajlović, Modeling thermal effects in braking systems of railway vehicles, Therm. Sci. 16 (2012) 515–526.
[38] M. Magelli, N. Zampieri, Q. Wu, Integration of brake block thermal equations within a railway vehicle multibody model: a multiphysics approach, Int. J. Real. Ther. (2024) 1–16.